The International Journal of Energy & Engineering Sciences, 2020, 5 (2) 80-104
ISSN: 2602-294X - Gaziantep University

DESIGN AND MODELLING OF INTERNAL PERMANENT MAGNET MOTOR

Muhammed Aslan, Ali Baran Özpolat, Cengiz İşçi, Fatih Eroğlu, Ahmet Mete Vural*

Electrical and Electronics Engineering, Gaziantep University, Gaziantep, Turkey.
Corresponding author e-mail: mvural@gantep.edu.tr

ABSTRACT

In this study, radial brushless motors with internal permanent magnet (IPM) is designed and modelled. These motors can be fed by alternating current (AC) or direct current (DC) sources. It is called permanent magnet synchronous motor when it is fed with an AC voltage, and brushless direct current motors when it is fed it with a DC voltage. Later on, design parameters of an electric motor that produces a torque of approximately 35 Nm, powered by a 72 V DC source is determined. Then, mathematical modeling is implemented based on the determined design parameters of permanent magnet electric motors. IPM motor's size, magnetic and thermal analyses are made by finite element analysis. Moreover, efficiency, torque and power of the designed IPM motor are calculated as the result of the analysis. Finally, it is revealed that the designed IPM motor has 24 slots and 8 poles and it has an efficiency of 92 %.

Keywords: Electric motors, Internal permanent magnet motors, Finite element analysis.

1. INTRODUCTION

Michael Faraday and Joseph Henry laid the foundations of electric motors that employ electromagnetic fields and the first real electric motor is invented by Thomas Davenport. Electric motors have started to gain popularity among researchers at 1830s and many variations have been proposed. However, commercial availability of electric motors begins in 1873 [1]. Electric motors can be powered by alternating (AC) current or direct current (DC). The mutual property behind working principle of all types of electric motors is employing electromagnetic fields. DC motors were developed first and have certain advantages and disadvantages. AC motors utilize two types of windings in it: primary and secondary. Primary winding is fed by AC grid power or a generator. Each motor has a stator which is composed of wound insulted wires or a permanent magnet. The rotor is placed mostly in the center, and it is affected by the magnetic field which is produced by the stator. Poles on the rotor are influenced by the stationary magnetic field created by stator poles and eventually, rotor starts to rotate. Insulated copper wires wound around the core are employed to generate or absorb electromagnetic energy. Utilization of copper wires in windings helps build motors with less size. Aluminum can also be utilized in windings but it must be able to carry the same amount of current in a safe manner. [2, 3]. Figure 1 shows two main types of electric motors as well as their subcategories [2, 4]. Table 1 summarizes the different aspects of different types of electric motors.

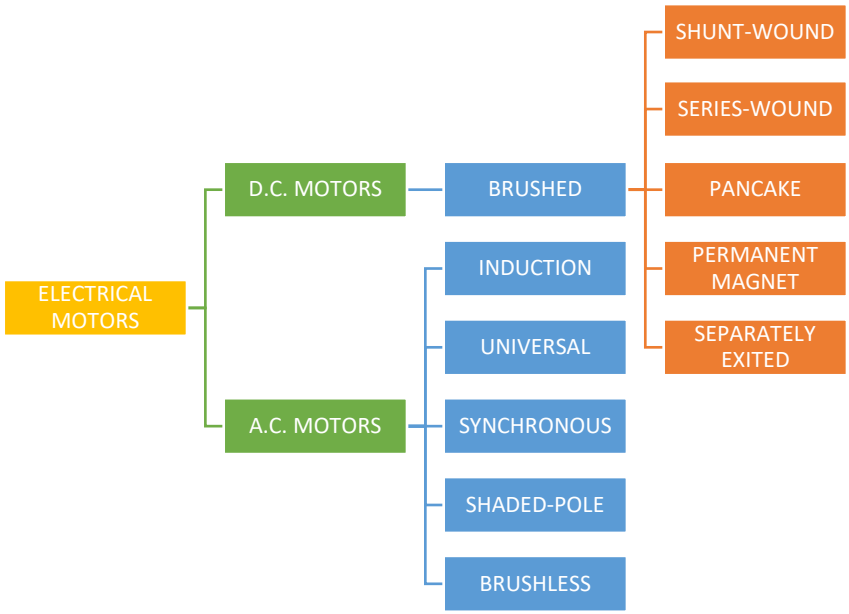

Figure 1. Types of electric motors.

Table 1. General properties of motors [5].

Property	DC motor	Squirrel cage asynchronous motor	Synchronous reluctance motors	Asynchronous reluctance motor with permanent magnet support	Permanent magnet synchronous motor
Cost	0	+ +	+	+	–
Moment/power density	–	0	0	+	+ +
Efficiency	–	+	+	+ +	+ +
Producibility	+ +	+ +	++	+	0
Controllability	+ +	+	0	+	+
Reliability	–	+ +	++	+	+
Dimension/mass/volume	–	+	+	+	+ +
Overloading capacity	–	+	+	+ +	+
Sturdiness	0	+ +	++	+	+
Field weakening ability	+ +	+ +	++	+ +	+
Error tolerance	+	+ +	++	+	–
Thermal limits	0	+	++	+	–
Lifespan	–	++	++	+	+
Maturity	++	++	+	–	+
Improvable	–	++	++	++	++

Brushed DC motors can be categorized in five different types as shown in Figure 1 [6, 7]. The DC shunt motor is constructed in a way that armature and field coil is connected in parallel and consequently voltages are the same for both windings. One advantage of DC shunt motors is the self-speed regulation ability. The DC series wound motor is a self-excited motor. The field winding and rotor winding are connected in series. DC series motors are advantageous in applications where high starting torque is necessary. A compound-wound motor is also a self-excited motor and utilizes both series and parallel connection of field windings. AC motors can be categorized in five different types as shown in Figure 1 [5]. The induction motor is the most popular electric motor in the industry which employs neither commutator nor brushes. It is used in modern diesel trains, industrial applications, pumps, and etc [8]. Being able to work at high operating speeds is the main advantage of induction motors. The Permanent magnet synchronous motor (PMSM) is very similar to the brushless DC (BLDC) motor, however, a sinusoidal feeding signal is employed to reduce torque ripple [9]. Organization of the multi-phase stator windings in a sinusoidal manner produces a flux density in sinusoidal form in the air gap. BLDC motors generate trapezoidal flux density and are different from PMSMs. In this paper, at first radial brushless motors with internal permanent magnets (IPM) are investigated. These motor types can work with both AC and DC supply. It is called as PMSM when it is fed with a sine voltage source, and BLDC motors when it is fed with a DC voltage source. Later on, an electric motor that produces a torque of approximately 35 Nm, powered by a 72 V DC source is designed. The proposed IPM motor is designed by determining within suitable magnetic limits.

2. INTERNAL PERMANENT MAGNET MOTORS

IPM motor is a type of motor that has a rotor embedded with a permanent magnet. Compared with the surface permanent magnet, IPM motor takes the advantage of reluctance torque and risk of a magnet being peeled off by centrifugal force is reduced. IPM motor allows various structures for embedding permanent magnets. IPM motor is more advantageous due to its ease of production and high efficiency. In this section, general features and types of IPM motor are explained. Figure 2 demonstrates the different types of IPM motors. The properties and advantages of IPM motors are as follows [10, 11, 12]:

- Compatibility with the same size of standard induction motor and easy replacement.
- Top efficiency level in all electric motor types.(Higher than IE3 level)
- Synchronous rotational speed, no slippage, hence more precise speed control.
- Standard inverter usage (IPM software must be installed).
- Balls can be replaced without removing the rotor.
- Less fan noise with smaller fan.
- High efficiency, energy saving with sharp reduction of losses.

- Suitable magnet position.
- The minimized losses compared to the standard induction motor thanks to being no loss in the rotor.

Properties of the material that is used in the IPM motor in this study are as follows:

- Stator lam model M400-50A is used.
- Stator lam back iron (5.734 kg) and for tooth (2.686 kg) are used.
- Rotor lam back iron (3.118 kg) and IPM magnet pole (3.247 kg) are used.
- N35UH magnets (0.756 kg) are used.
- Relative permeability of the magnet is 1.05.
- Magnetic flux density (Br) is 1.21 Tesla
- Electrical resistivity of the magnet is 1.8E-06
- Coercivity (HcB) of the magnet is 907 kA/m
- Maximum operating temperature of the magnet is 180 ºC.

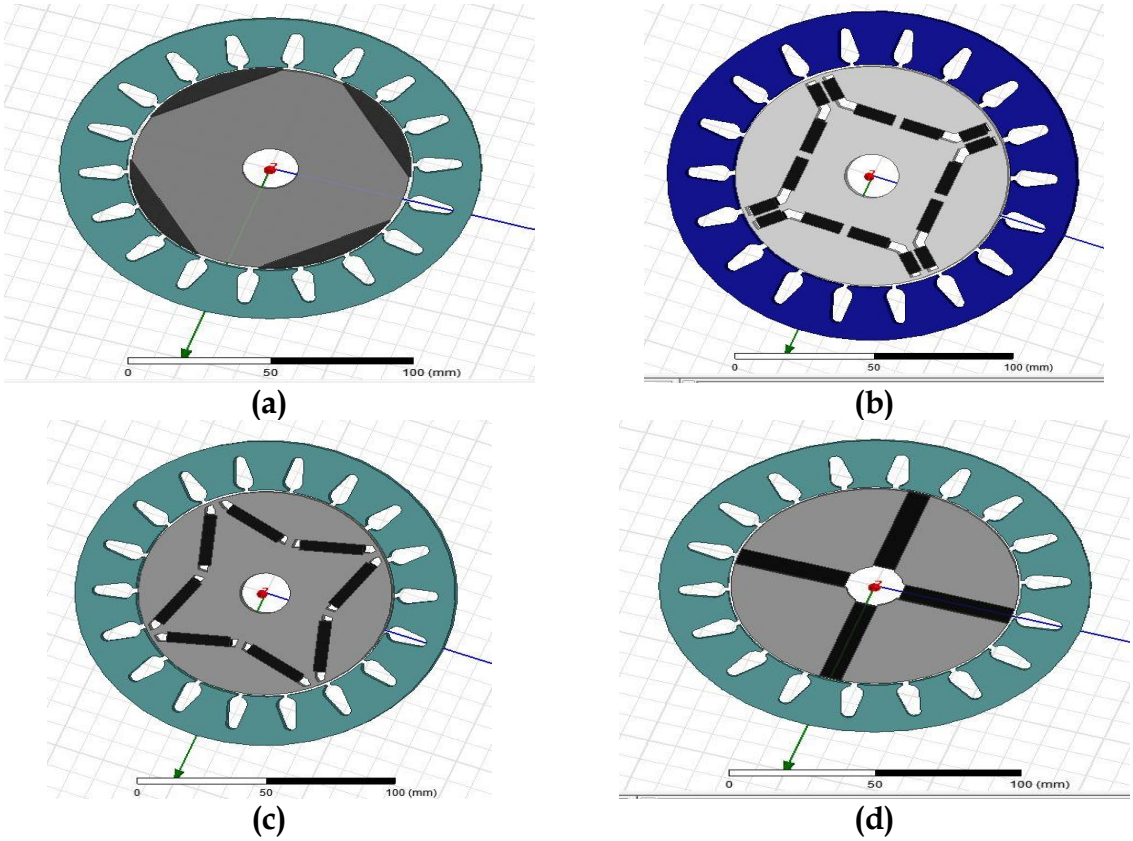

Figure 2. Different types of IPM motors, (a) Surface permanent magnet motor, (b) Embedded IPM motor, (c) V shape magnet embedded IPM motor, (d) Inserted IPM motor.

In the next section, mathematical analysis of IPM motors will be given.

3. MATHEMATICAL ANALYSIS

3.1 Introduction

The mathematical analysis and modelling are key to understand the effects of parameters on the outcome of the system. This section analyzes and explains the formulas that are used in the modelling the IPM motor.

3.2 Force equations

In this part, it is aimed to find the total force, since the designed motor is for an electrical bicycle. Firstly, the motor should carry the vehicle across to the air resistance. Formula for air resistance is given below [13];

$$Fa = C \times S \times \frac{\rho}{2} \times \frac{{V_r}^2}{3600} \tag{1}$$

where C is the coefficient of air-resistance/nose form factor, S is the cross-sectional windward area in terms of meter square, ρ is the air density in terms of kilogram per meter square and V_r is the velocity of the bike relative to the wind velocity in terms of kilometer per hour. Secondly, the rolling resistance should be considered in the force calculations. The rolling resistance is calculated by the given formula [13];

$$Fr = f_c \times m \times g \times \cos\alpha \tag{2}$$

where f_c is the coefficient of rolling-resistance, m is the mass of whole bike in terms of kilogram, g is the gravitational constant in terms of meter over area square and α is the slope angle. The climbing resistance which is the resistance that have a relationship between mass in terms of kilogram, gravitational constant in terms of meter over area square and a as slope angle can be calculated as follows [13];

$$Fg = m \times g \times \sin\alpha \tag{3}$$

Acceleration force is related to mass in terms of kilogram and the distance in terms of meter;

$$Fm = m \times x \tag{4}$$

where $x = dV/dt$.

The total force can be found by summing all forces;

$$Ft = Fa + Fr + Fg + Fm \tag{5}$$

Finally, after calculating the total force, for a rated speed of 350 rpm, the required power and torque of IPM are found as 1282 W and 35.91 Nm, respectively by using the parameters given in Table 2.

Table 2. Parameters for torque and power calculations.

Parameter (Unit)	Value
C (No unit)	0.6
S (m^2)	0.5
ρ (kg/m^2)	1.326
V_r (km/h)	40
f_c (No unit)	0.0112
m (kg)	112
g (m/s^2)	9.81
α (degree)	0

3.3 Magnetic modeling

Operation of brushless permanent magnet motor is based on the conversion of energy from electrical to magnetic and magnetic to mechanical. It is really necessary to formulate the methods for computing the torque as the magnetic energy plays a key role in this formulation. Here, it is significant to determine the magnetic field distribution within the motor as it has a direct effect on magnetic energy.

Two vector quantities, namely, flux density B and field intensity H, describe a magnetic field. The relationship between B and H is described as follows:

$$B = \mu \times H \tag{6}$$

where μ is the permeability of the material.

The flux density which passes through a specific area is called as magnetic flux. It is written as

$$\Phi = B \times A \tag{7}$$

where A is the cross-sectional area of the material.

The total change in the magnetic field intensity due to distance is called magnetomotive force. It is described as;

$$F = H \times l \tag{8}$$

where l is the length.

The ratio of Φ and F give the magnetic permeance, which is given by [13];

$$P = \frac{\mu \times A}{l} \tag{9}$$

By using P, reluctance can be found as [14];

$$R = \frac{1}{P} \tag{10}$$

Up to now, the basic equations are explained in this part. Now, it is time to explain other magnetic relationships by using those equations. In all motors, flux is passed through air gap between the rotor and stator. Hence, permeance or reluctance of the air gap should be modelled. Air gap permeance can be calculated for many applications using the formulation given below [14];

$$Pg = (\mu_0) \times \left(\frac{A}{lg_e}\right) \tag{11}$$

where l_{ge} is the effective air gap length. It is described as;

$$lg_e = K_c \times lg \tag{12}$$

where K_c is the Carter's coefficient and g is air gap length. The Carter's coefficient is a parameter that can be used to estimate the contracted or effective slot pitch in case of armature with open or semi enclosed slots [14]. The parameter K_c is given as;

$$K_c = [1 - \frac{1}{\frac{\tau_s}{w_s} \times (\frac{5 \times lg}{w_s} + 1)}]^{-1} \tag{13}$$

where τ_s is distance among two magnets and ω_s is distance among two teeth in the slot. When the air gap permeance is found, it is easy to find air gap reluctance. The fact that flux does not flow through the air gap straightly makes modelling the permeance of air gap P_g. This is because the air in the gap has the same permeability as the air near the gap, hence some of the flux fringes into the air near the gap. Those fringes create the fringing permeance which is given below [14];

$$Pf = (\frac{\mu_0 \times L_d}{\pi}) \times \ln\left(1 + \frac{\pi \times X}{lg}\right) \tag{14}$$

where L is the deep length of the block into the page and X is the extent that the fringing permeance extends up the sides of the blocks. Magnet permeance is formulized as

$$P_m = \frac{\mu \times A_m}{l_m} \tag{15}$$

where A_m is the cross-sectional area of the magnet and l_m is the thickness of the magnet. Ratio of the magnet length to the air gap length and the flux concentration factor determine the permeance coefficient as

$$P_c = \frac{l_m}{lg \times C_\Phi} \tag{16}$$

where C_Φ is the flux concentration factor, defined as

$$C_\Phi = A_m / A_g \tag{17}$$

where A_g is the cross-sectional area of the air gap.

For safe operation of the magnet, permeance coefficient must be greater than one and the length of the magnet must be significantly larger than the air gap length. Furthermore, increasing the air gap flux density through flux concentration, where C_Φ>1, results in lower permeance coefficient. After determining equations (16) and (17), air gap flux density can be found as [14];

$$B_g = \frac{K_l \times C_\Phi}{1 + \frac{K_r \times \mu_r}{P_c}} \times B_r \tag{18}$$

where K_l is the leakage factor, Kc is the reluctance factor and Br is the remanence. For the motor being considered here with surface magnets, the leakage factor is typically in the range $0.9<K_l<1.0$, the reluctance factor is in the range $1.0<K_r<1.2$, and the flux concentration factor is ideally 1.0. If these values and the remanence B_r are considered to be fixed by the selection of magnet, amplitude of the air gap flux density is determined by the permeance coefficient P_c. As the permeance coefficient increases, the air gap flux density approaches a maximum that is slightly less than the remanence. It is impossible to achieve an air gap flux density B_g which is greater than B_r without flux concentration. Moreover, there is a nonlinear relationship between air gap flux density and permeance coefficient. The air gap flux density approaches the remanence asymptotically. Doubling P_c does not mean double B_g. However, doubling P_c doubles the magnet length, which means doubling the cost and volume.

The remanence is the maximum flux density that the magnet can produce by itself. It is easily affected by temperature. It is described as [14];

$$B_r(T) = B_r(T_0) \times [1 + \Delta B \times (T - T_0)] \tag{19}$$

where T is the magnet temperature, T_0 is a reference temperature, $B_r(T_0)$ is the remanence at T_0, and ΔB is the reversible temperature coefficient.

3.4 Coil Resistance And Coil Inductance

Multiple coils are connected together to generate phases in motors. Coils have their own resistance and inductance. Among these parameters, inductance is harder to model especially when mutual inductance is present. In general, material resistivity is a function of temperature and there is an exponential relationship between them as expressed below [14];

$$\rho(T) = \rho(T_0) \times [1 + \alpha_t \times (T - T_0)] \tag{20}$$

where T is the temperature, T_0 is the reference temperature and α_t is the thermal resistivity coefficient. The use of slots constraints basically in order to hold the coils places on motor design. Therefore, slot calculations should be considered. In order to find the slot resistance, firstly, slot fill factors should be indicated. The bare wire slot fill factor is defined as [14];

$$K_{wb} = \frac{N \times A_{wb}}{A_S} \tag{21}$$

where N is the number of the turn, A_s is the cross-sectional area of the slot and A_{wb} is the bare wire cross-sectional area. A_{wb} can be described as [14];

$$A_{wb} = \frac{W_{th}}{d_s} \tag{22}$$

where d_s is tooth length and w_{th} is the width of the slot. After defining the slot fill factor, it is time to describe the slot resistance as [14];

$$R_S = \frac{\rho(T) \times l \times N^2}{K_{wb} \times A_s} \tag{23}$$

Inductance is not usually a critical parameter in brushless permanent magnet motors. The time constant of the windings, and consequently, the rate of change of winding currents are determined by inductance, given as follows;

$$L_i = \frac{\Lambda}{i} \tag{24}$$

where

$$\Lambda = \frac{N^2 \times i}{R} \tag{25}$$

In addition to self-inductance as described above, mutual inductance exists between the coils in a given phase as well as between the coils in different phases, but mutual inductance between coils in a given phase is considered here, because mutual inductance between phases is small relative to self-inductance. When coils are placed in slots, the coil inductance has three distinct components due to the three distinct areas where significant magnetic field is created by coil current. These three areas are the air gap, the slots, and the end turns as described below [14];

$$L_g = \frac{2\pi \times \mu_0 \times l \times R_{r0}}{1 + \frac{l}{\mu_r \times C_\Phi}} \times Nc^2 \tag{26}$$

$$L_s = N_m \times (2 \times N_c)^2 \times \left[\frac{\mu_0 \times d_s \times l}{3 \times w_{sb}} + \frac{\mu_0 \times d_t \times l}{\frac{w_{so} + w_{sb}}{2}} + \frac{\mu_0 \times d_{sh} \times l}{w_{so}} \right] \tag{27}$$

$$L_e = \frac{N_m \times \mu_0 \times \tau_{cp} \times N^2}{2} \times \ln\left(\frac{\tau_{cp} \times \sqrt{\pi}}{\sqrt{2 \times A_s}}\right) \tag{28}$$

where N_c is conductor number, N_m is the number of magnets, l is the length of the motor, R_{ro} is air gap radius, dt is distance between tooth and entrance, d_{sh} is the thickness of the slot entrance, w_{sb} is slot width and w_{so} is entrance of the slot width. After determining equations (26), (27) and (28), the net phase winding inductance can be found in series as [14];

$$L_{ph} = L_g + L_s + L_e \tag{29}$$

3.5 Back EMF and torque

An important disadvantage regarding BLDC motors is the generated back EMF by its windings. The back EMF induced in the BLDC motor is directly proportional to the speed of the rotor and field strength of the motor. The produced back EMF behaves like a resistance, so if the speed of the DC motor or field strength is increased, the back EMF increases which consequently increases the resistance to the current flow in windings. Therefore, current delivered to the armature is reduced.

The back EMF is formulized as follows:

$$E_b = K_e \times w_m \tag{30}$$

where ω_m is mechanical angular speed and K_e is back EMF constant. K_e is also described as

$$K_e = 2 \times N_c \times B_g \times l \times R_{ro} \tag{31}$$

Thus, torque can be expressed by using (30) and (31)

$$T = \frac{E_b \times i}{w_m} = K_e \times i \tag{32}$$

where i is current. Also, (32) confirms that $T = K_e \times D^2 \times l$ where D is the rotor diameter. Since the torque constant and back EMF constant vary with N and the product Ni is constant, they are not good indicators of motor performance. A more useful performance indicator is the motor constant, given as follows;

$$K_m = \frac{B_g \times R_{ro}}{\sqrt{\rho(T)}} \times \sqrt{V_{wb}} \tag{33}$$

where V_{wb} is the bare wire volume contained in the two slots. The motor constant defines torque efficiency which is nothing but how efficiently a motor produces torque as a function of the load losses. Hence, motor constant does not only depend on the desired motor output, but is also inversely proportional to the cost that occurs while generating the corresponding output. The torque per unit rotor volume describes the amount of torque available from a given rotor volume. As such, it is a common measure for comparing motors and for initial motor sizing for a given application. It is defined as

$$T_v = \frac{2 \times N_m \times B_g \times N \times i}{\pi \times R_{ro}} \tag{34}$$

3.6 Energy and power calculations

The stored energy in a magnetic field is a significant quantity as the magnetic field is the medium through which electric energy is converted to mechanical energy. Furthermore, energy stored in a magnetic field is a key parameter in the design. It can be defined as [14];

$$W = \frac{\lambda^2}{2 \times L_i \times i} \tag{35}$$

where L_i is the inductance. When ferromagnetic materials are excited, energy is dissipated due to hysteresis and eddy current losses. These losses are generally combined and called core losses. Hysteresis loss occurs due to hysteresis loop causes an energy loss. The hysteresis power loss is described by

$$P_h = k_h \times f \times B^n \tag{36}$$

where k_h is a constant that depends on the material type and dimensions, f is the frequency of applied excitation, B is the flux density amplitude within the material, and n is a material dependent exponent usually between 1.5 and 2.5. Electric currents induced within the ferromagnetic material generate eddy current. Induced eddy currents result in power losses due to the resistive property of the material. This loss can be explained by the relationship

$$P_e = k_e \times h^2 \times f^2 \times B^2 \tag{37}$$

where h is the material thickness and k_e is a material dependent constant. The easiest way to reduce eddy current loss is to increase the resistance in the material. This is commonly done in a variety of ways. As described by the equation (37), eddy current loss is proportional to the square of the lamination thickness. Thus, thin laminations should be used to achieve lower losses at high frequencies. Up to now, formulas related to inner motor structure was studied. Now, it is time to study about general structure of motor formulas and indicated the efficiency. Firstly, the mechanical power is given below by using (32)

$$P_m = T \times w_m \tag{38}$$

The required total power is given below by using (5) [14];

$$P_t = F_t \times V \tag{39}$$

In (39), V can be calculated by the following equation [14];

$$V = \frac{V_{r0} \times 1000}{3600} \tag{40}$$

where V_{r0} is the velocity of revolutions per minute. Thus, by using (39), the required total torque can be defined as [14]

$$T = \frac{P_t}{\frac{V_r \times 2 \times \pi}{60}} \tag{41}$$

After calculating the required powers, by using (36), (37), (38) and (39), the efficiency can be calculated as follows;

$$\eta = \frac{P_m}{P_m + P_t + P_e + P_h} \tag{42}$$

4. INTERNAL PERMANENT MAGNET MOTOR DESIGN WITH INFINITE ELEMENT METHOD

In this section, the IPM motor is designed by using MotorCAD package program.

4.1. IPM motor dimensional design with MotorCAD

MotorCAD is Computer Aided Design (CAD) package for the design of electric motors. MotorCad analysis flow chart is illustrated in Figure 3.

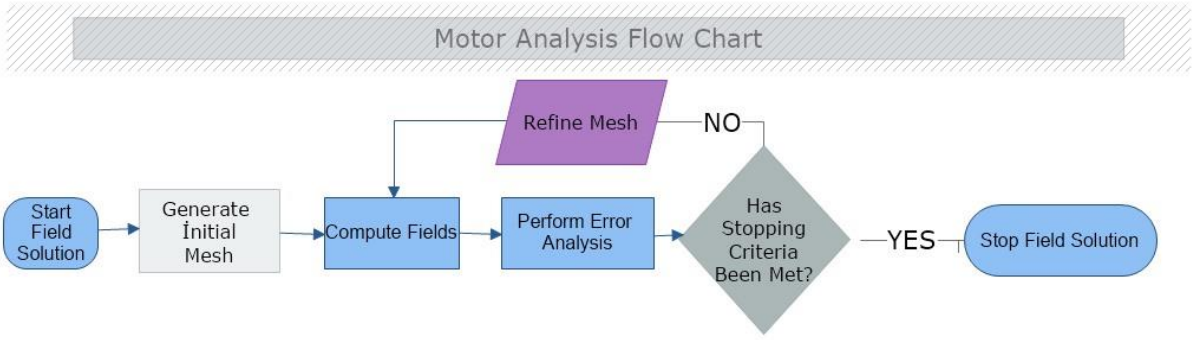

Figure 3. MotorCad analysis flow chart.

Using the formulas presented in the previous section, the radial and axial lengths of the IPM motor are defined in MotorCAD. The final stator and rotor side radial dimensions as well as motor axial dimensions are presented in Table 3, Table 4, and Table 5, respectively.

Table 3. Stator radial dimensions.

Stator Parameter	Value	Unit
Slot Type	Parallel Tooth	
Stator Ducts	None	
Slot Number	24	
Stator Lamination Diameter	185	mm
Stator Bore	122	mm
Tooth Width	6	mm
Slot Depth	18,50	mm
Slot Corner Radius	2	mm
Tooth Dip Depth	2	mm
Slot Opening	2	mm

Table 4. Rotor radial dimensions.

Rotor Parameter	Value	Unit
Rotor Type	Interior V(Web)	
Pole Number	8	mm
Magnet Thickness	3	mm
Magnet Bar Width	20	mm
Bride Thickness	1	mm
Web Thickness	4	mm
Web Length	2	mm
Pole V Angle	124	o
Pole Arc	150	o
Air Gap	1	mm

Table 5. Motor axial dimensions.

Motor Parameter	Value	Unit
Motor Length	180	mm
Stator Lamination Length	110	mm
Magnet Length	105	mm
Magnet Segment	3	-
Rotor Lamination Length	105	mm

As seen in the above tables, there are 24 slots and 8 V type magnets in the IPM motor. Employing 24 slots and 8 magnets slightly increase the knock torque, but simplify the winding shape. Radial, axial and three-dimensional views of the IPM motor are shown in Figure 4. Next, magnetic analysis, steady-state and transient solution analysis, and thermal analysis will be held to see if the designed motor is ideal or not. Before starting the analysis, coil winding scheme and the grooves should be filled according to the coil diameter that is used. Then analysis conditions need to be determined. Analysis can be initiated by entering the maximum current, speed and power parameters in the calculation section.

4.2. IPM motor winding design with MotorCAD

Industrial electric motor manufacturing companies want to obtain electric motor with maximum power and efficiency while designing. Hence, winding scheme is very important to achieve this ratio. They want the end of the winding to be as short as possible, with the winding being quick and easy.

Table 6. Winding parameters of the IPM motor.

Winding Parameter	Value
Phases	3
Turns	6
Throw	5
Parallel Path	2
Winding Layer	1

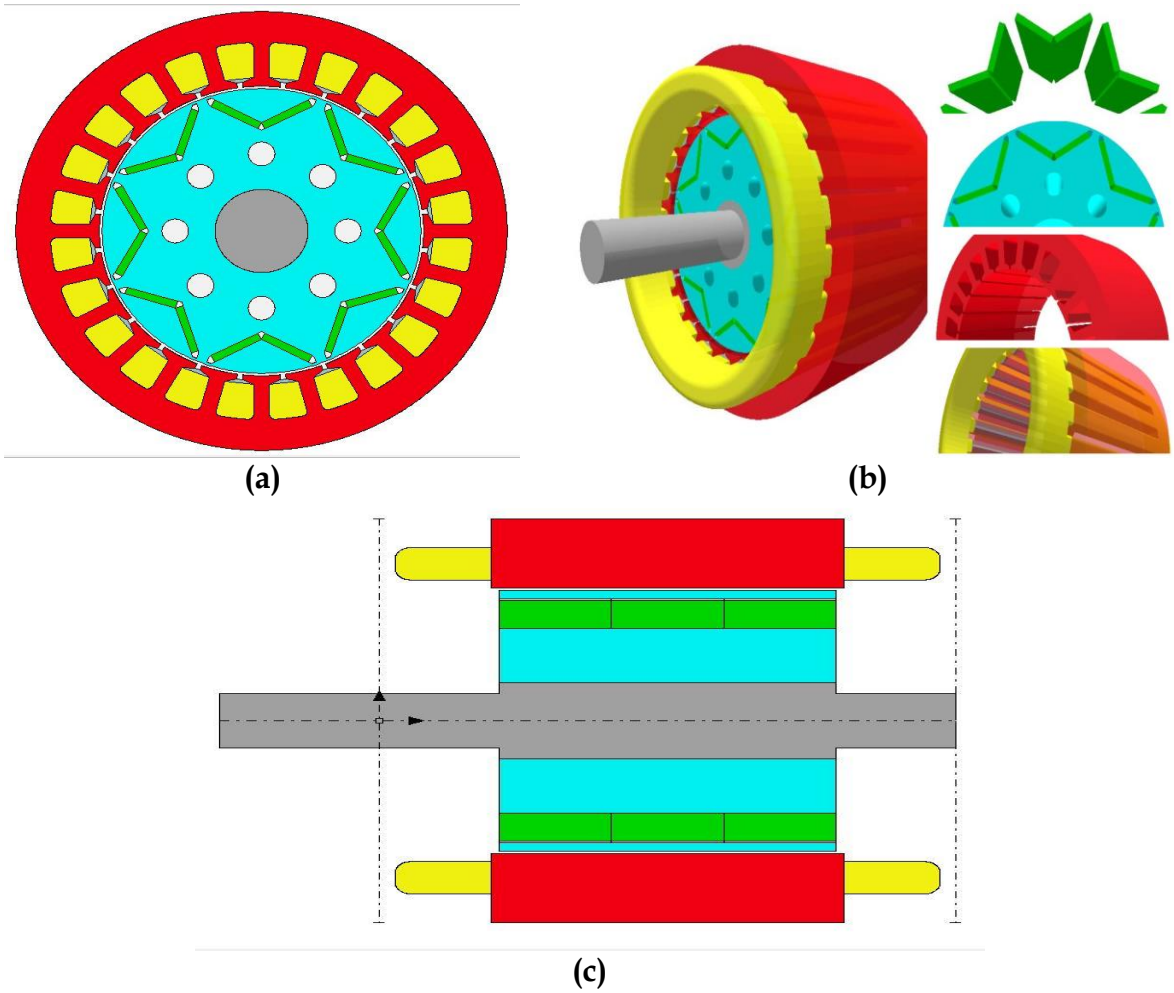

Figure 4. Radial, axial and three-dimensional views of IPM motor: (a) Radial aspect of motor 2D, (b) Aspects of 3D motor shape (Red: Stator, Yellow: Coil, Blue: Rotor, Green: Magnets), (c) Axial aspect of motor 2D.

In order to make the winding easier, the gutter magnet ratio is determined as the exact fraction (24/8 = 3). The winding diagrams offered by the program according to this sizing design are given in Table 6. Before starting the simulations, mechanical MMF harmonics and winding factors are analyzed analytically based on the winding pattern in Figure 5. The diameter of the copper wire has been determined as 0.5 mm. The coils were made in parallel with the diameter to carry the maximum currents. 53.39 percent of occupancy was caught in the groove. Fine selection of copper wire facilitates winding. In addition, hysteresis increases losses, however these losses are tolerable.

4.3. IPM motor calculation parameters and magnetic solutions with MotorCAD

In the calculation part, the input and boundary parameters are defined. All solutions on steady-state condition are calculated using MotorCAD. General calculation parameters of the designed IPM motor are given in Table 7.

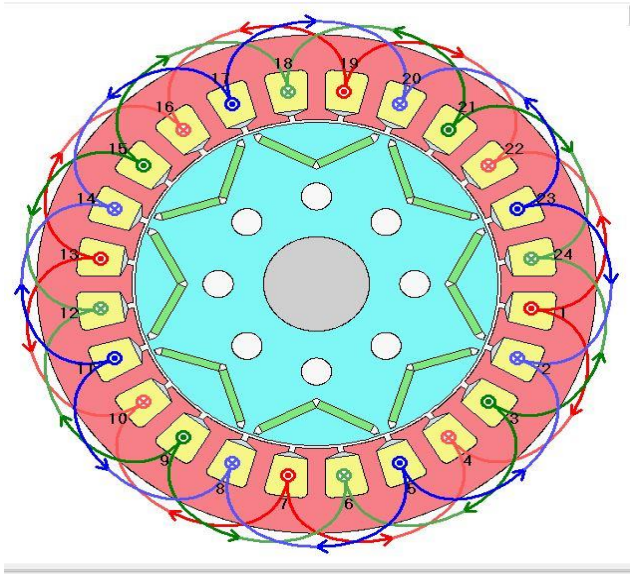

(a)

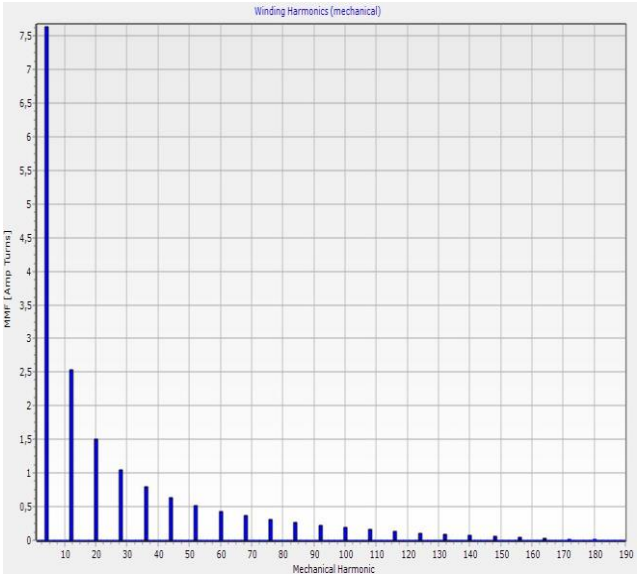

(b)

Wire Selection

Wire Type: Metric Table

Wire Gauge: Diameters - [0,543mm, 0,475mm]

Input Parameter	Value
Wire Slot Fill	0,78
EWdg Fill	0,7798
Liner Thickness	0,25
Copper Depth [%]	100
Conductor Separation	0,01

Input Parameter	Value
Number Strands in Hand	50
Conductors/Slot	600
EWdg MLT	177,517

Output Parameter	Value
Wire Slot Fill (Wdg Area)	0,78
Wire Slot Fill (Slot Area)	0,6977
Copper Slot Fill (Slot Area)	0,5339
Heavy Build Slot Fill	0,9932
Winding Depth	14,626
Conductors/Slot Drawn	600

Output Parameter	Value
Slot Area	199,2
Winding Area (+Liner)	188,6
Winding Area	178,1
Covered Wire Area	138,9
Copper Area	106,3
Impreg Area	39,19
Wedge Area	10,57

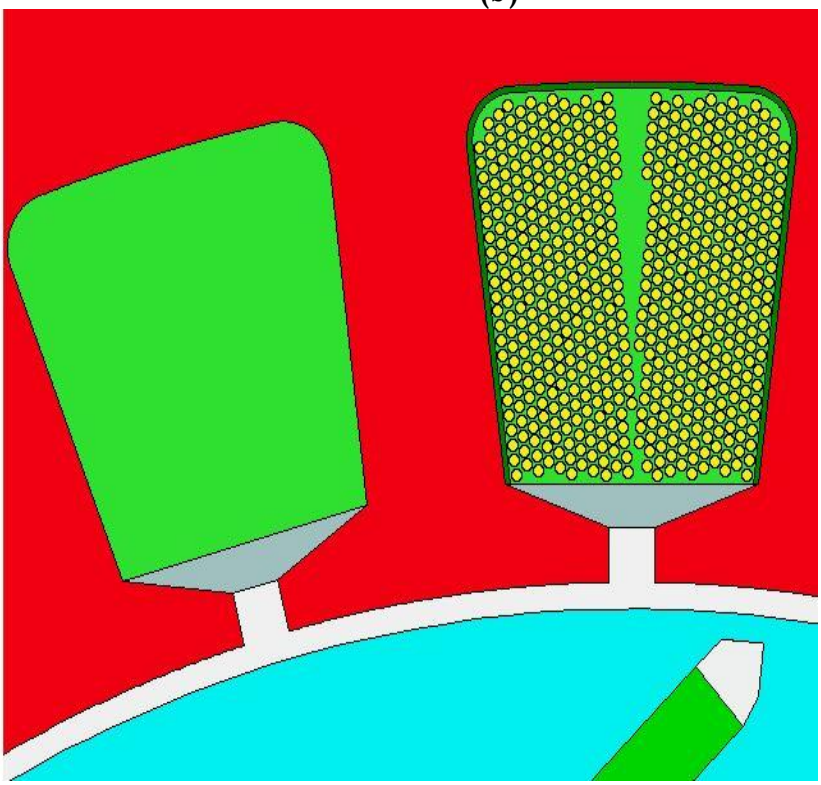

(c)

Figure 5. Winding simulations of IPM motor; (a) Winding schema of IPM motor with MotorCAD, (b) Winding harmonics of IPM motor with MotorCad, (c) Winding aspect of IPM motor with MotorCAD.

Table 7. Parameters of the IPM motor with MotorCAD

Input Parameter	**Value**
Shaft Speed (RPM)	600
Line Current Definition	Peak
Peak Current (A)	40
Dc Bus Voltage (V)	72
Phase Advance (Degree)	45
Drive Mode	Sine
Armature Winding Temperature (ºC)	60
Magnet Temperature (ºC)	80

For common electrical steels, hard saturation is reached at a flux density between 1.7 and 2.3 T and the onset of the saturation occurs in the neighborhood of 1.0 and 1.5 T. Therefore, magnetic flux density should be observed especially at the tooth deep on the stator. If the magnetic flux density is bigger than 2.3 T, geometry model and winding parameters should be redefined. Besides, as seen in Figure 6 that the magnetic flux density never passes 1.8 T. Figure 6 also demonstrates the steady-state analysis of IPM motor.

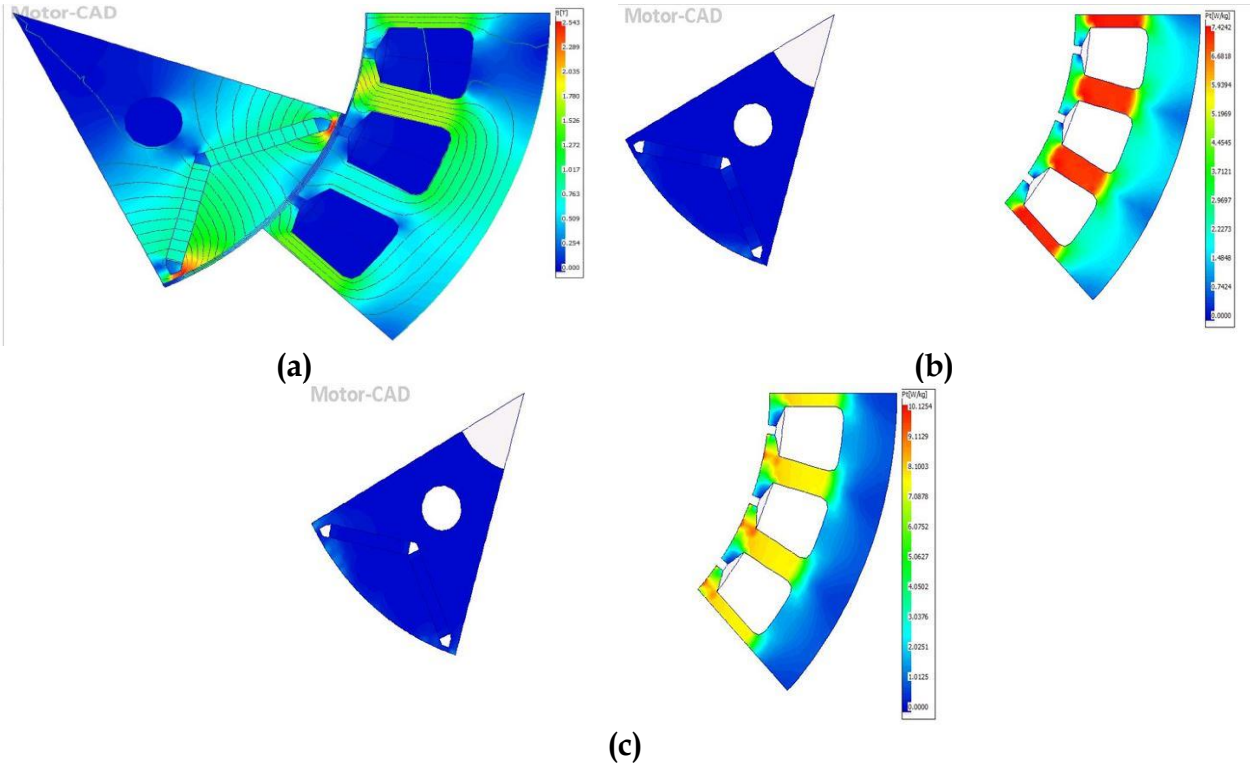

Figure 6. Steady-state analysis of IPM motor; (a) Magnetic flux densities, (b) Open circuit loss, (c) Total loss on load.

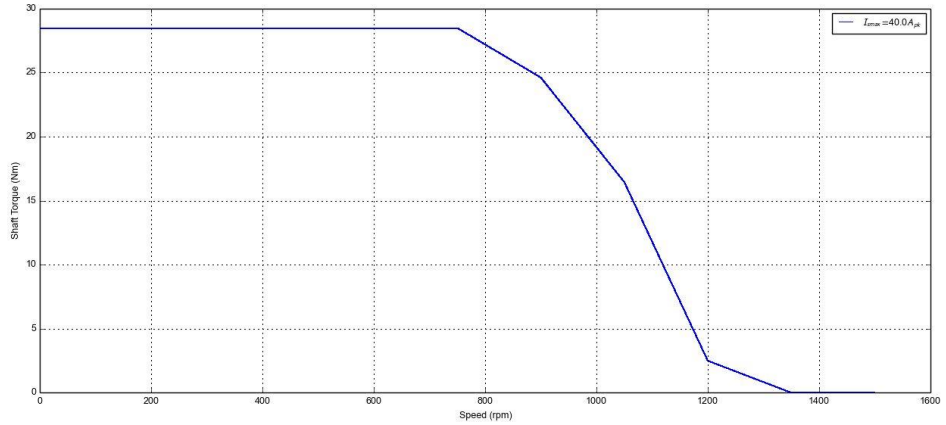

(a)

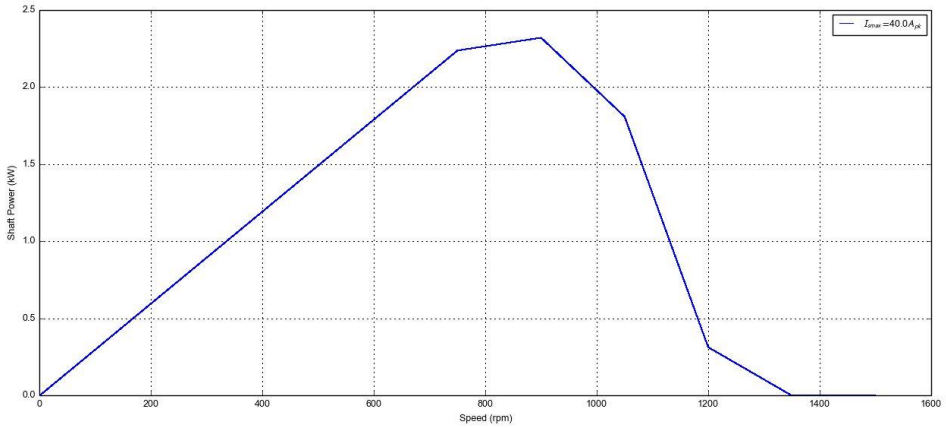

(b)

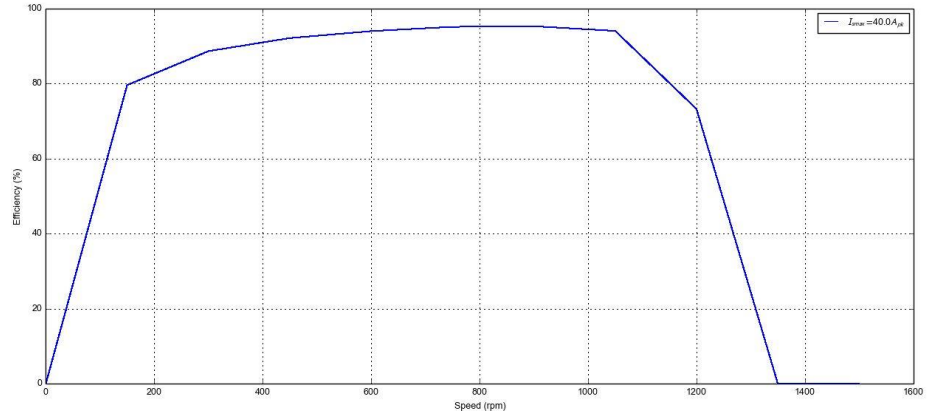

(c)

Figure 7. Further analysis of IPM motor; (a) Speed-torque curve (rpm-Nm), (b) Speed-power curve (rpm-kW), (c) Speed-efficiency curve (rpm-%).

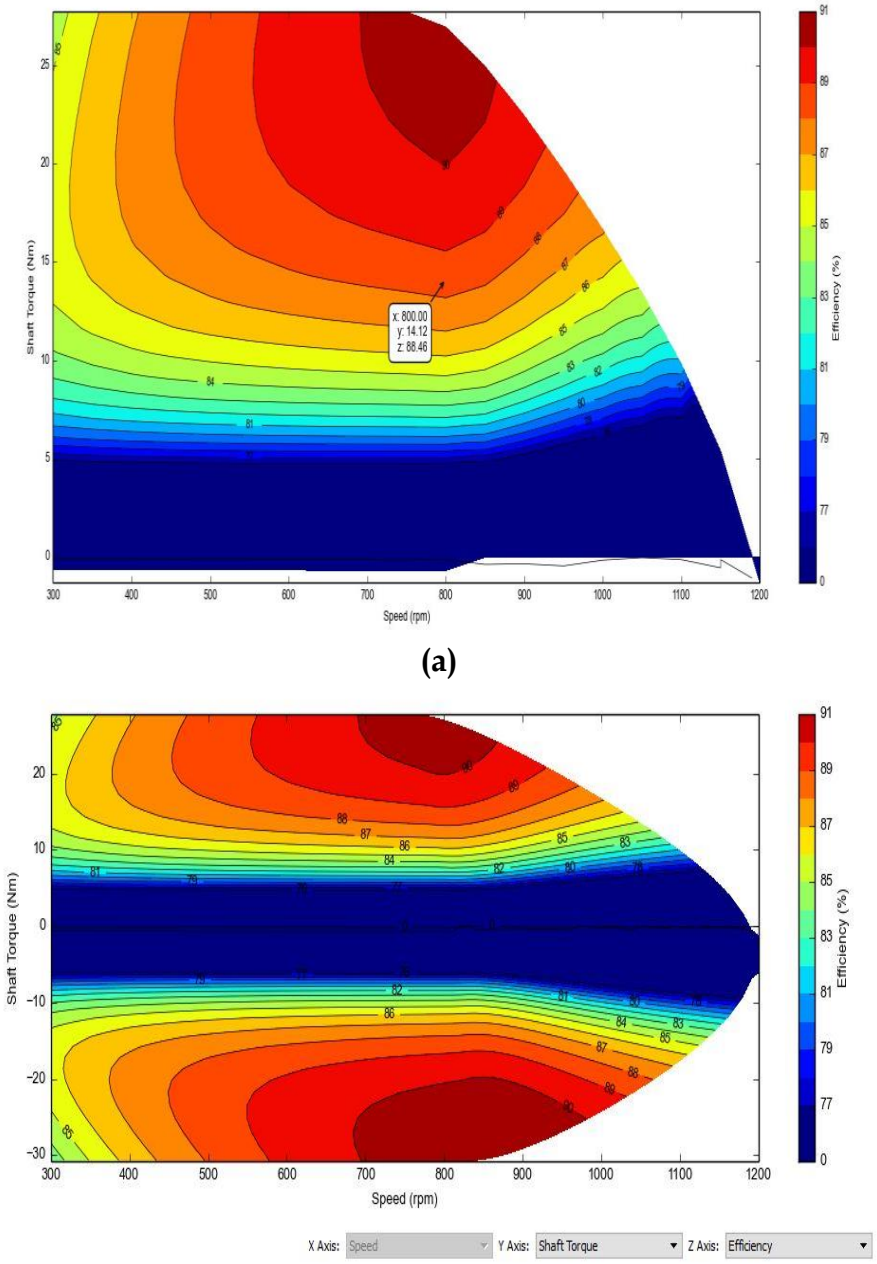

(a)

(b)

Figure 8. Speed-torque (rpm-Nm) and speed-efficiency (rpm-%) curves of the IPM motor: (a) Motor, (b) Motor and generator.

It should be noted that DC bus voltage is different from Back-EMF Voltage. It is desired to make DC bus voltage closer to Back-Emf to decrease losses, but DC bus voltage should be always bigger than Back-EMF. This is because when Back-EMF is bigger than DC bus, this machine becomes a generator. Motor constant parameters that are needed to drive the circuit are given in Table 8. As seen, this permanent magnet BLDC motor generates a maximum of 40 Nm of torque and 1.5 kW of output power. It is concluded that a bicycle or some other low powered vehicles can be driven with this

motor. Finally, it is calculated using MotorCad that the efficiency of the designed motor is 91.587 % at the steady-state condition. All those solutions indicate that the initial design is good enough to continue to the design. Further analysis on IPM motor can be observed in Figure 7 and 8.

Table 8. All solution data of IPM motor at steady-state condition using MotorCAD.

Variable	**Value**	**Unit**
Airgap Flux Density (Mean)	0.5441	Tesla
Airgap Flux Density (Peak)	0.951	Tesla
Stator Tooth Flux Density (Peak)	1.737	Tesla
Stator Tooth Tip Flux Density (Peak)	1.582	Tesla
Stator Back Iron Flux Density (Peak)	0.78	Tesla
Rotor Back Iron Flux Density (Peak)	*0.2077*	Tesla
DC Bus Voltage	*72*	*Volt*
Line-Line Supply Voltage (RMS)	50.91	Volt
Phase Supply Voltage (RMS)	29.39	Volt
Back-EMF Line-Line Voltage (RMS)	*60.4*	*Volt*
Back-EMF Phase Voltage (RMS)	23.4	Volt
Line Current (Peak)	40	Amper
Phase Current (RMS)	28.28	Amper
D-axis and Q-axis Inductance	0.893-1.868	mH
Torque Constant (Kt)	0.6249	Nm/A
Motor Constant (Km)	2.335	Nm/(Watt^0.5)
Back-EMF Constant (Ke)	0.9613	Vs/Rad
Short Circuit Line Current (Peak)	137.6	Amper
Short Circuit Max. Demagnetize Current	-267.2	Amper
Fundamental Frequency	40	Hz
Maximum Available Torque	*30*	*Nm*
Cogging Torque	*3.6*	*Nm*
Speed Limit for Constant Torque	870	Rpm
Input Power	1685	Watt
Output Power	1543.3	Watt
Total Loss (On Load)	141.76	Watt
System Efficiency	91.587	%
Torque Per Rotor Volume	21.048	kNm/m^3

4.4. Thermal analysis and final output data with motor cover

Motor cover design is very important for the design of the cooling system. Perfect cover design decreases the temperature in the system and protects it from external impacts. A water jacket cover design within the MotorCad is used in this paper. This is an active cooling system with the shape of water channel. The designed system is

able to maintain the temperature stable and increases performance of the system. Motor cover is made by stainless steel as shown in Figure 9. Another issue is to monitor the temperature of the system at all points at steady-state and transient solutions. If the magnet temperature is bigger than 90 Celsius degrees, the magnets will demagnetize. Hence, one has to be careful and should use thermostat to stop the motor while passing this critical temperature point. Moreover, the thermal analysis solution and thermal losses at steady-state and transient solutions are given in Table 9, Table 10, and Figure 10, respectively. Table 11 shows all solution data for IPM Motor at transient condition. It can be said that IPM motor is available for all conditions but optimization is required because the knock torque is high.

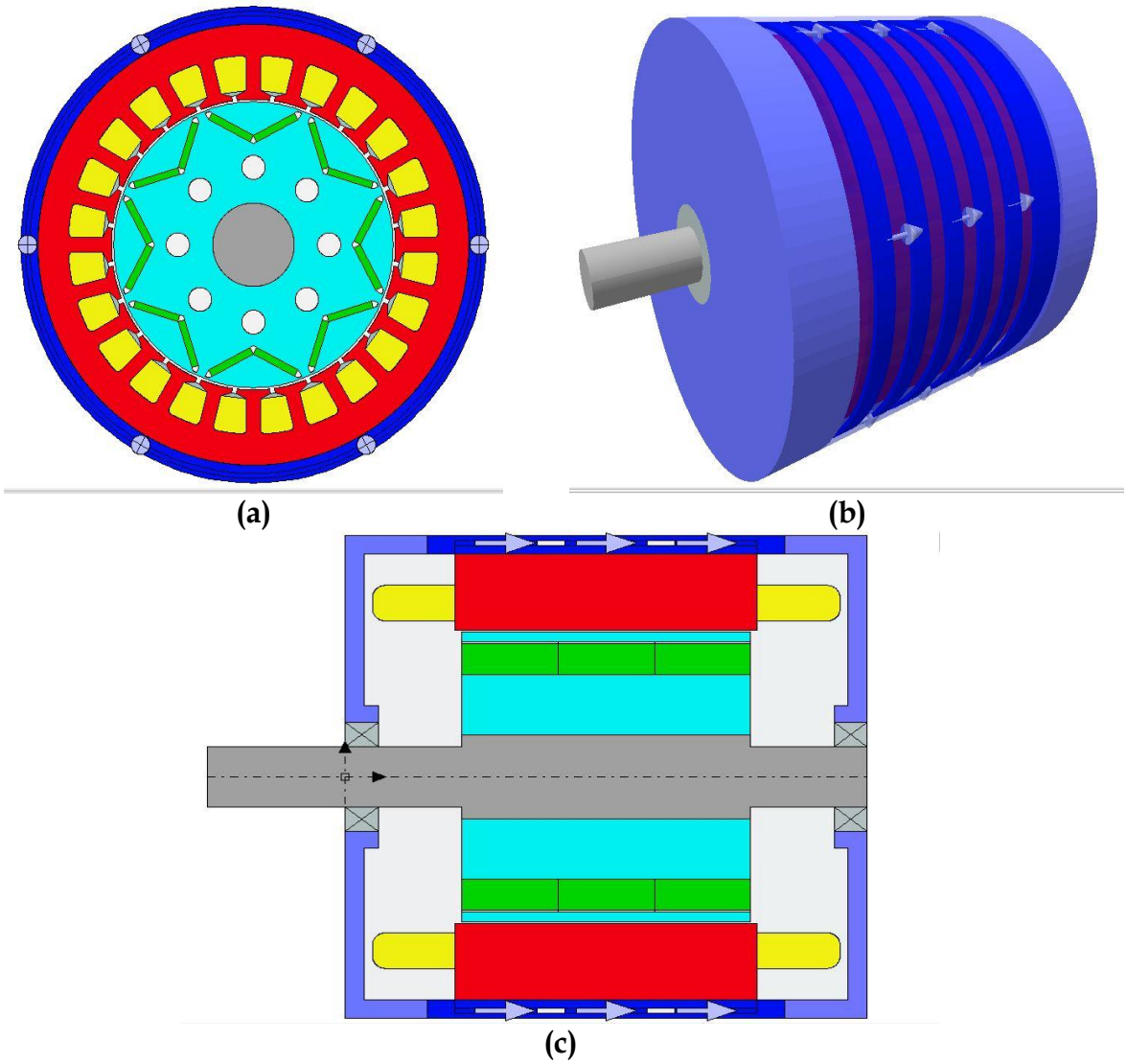

Figure 9. Different views of IPM motor with water jacket cover: (a) Radial view, (b) 3D view, (c) Axial view.

Table 9. Losses with thermal solution for transient analysis.

Variable	Value	Unit
Armature DC Copper Loss (On Load)	245.7	Watts
Magnet Loss	0.04552	Watts
Stator Iron Loss [Total] (On Load)	43.83	Watts
Rotor Iron Loss [Total] (On Load)	1.699	Watts
Total Losses (On Load)	291.3	Watts
Stator Back Iron Loss (On Load)	7.14	Watts
Stator Back Iron Loss [Eddy] (On Load)	2.097	Watts
Stator Tooth Loss [Hysteresis] (On Load)	28.35	Watts
Stator Tooth Loss [Eddy] (On Load]	5.534	Watts
Stator Tooth Loss Total	34.54	Watts
Stator Iron Loss Total (On Load)	43.83	Watts

Table 10. Temperatures of different IPM motor parts.

IPM Motor Part	Max Degree (°C)
Housing (Blue)	82.2
Magnets (Green)	88.6
Rotor Surface (Magenta)	88.7
Shaft Centre (Grey)	88.3
Stator Surface(Red)	89.4
Stator Yoke (Red)	85
Tooth (Red)	87.5
Winding Average (Yellow)	93.7

Table 11. All solution data of IPM motor at transient condition with MotorCAD.

Variable of IPM Motor	Value	Unit
Maximum Torque Possible	45	Nm
Average Torque (Virtual Work)	31	Nm
Torque Ripple	10	Nm
Speed Limit For Constant Torque	997	Rpm
Electromagnetic Max. Power Limit	3288	Watts
Input Power	3534	Watts
Output Power	3243	Watts
Total Losses (On Load)	291	Watts
System Efficiency	91.758	%
Torque Per Rotor Volume	26.645	kNm/m^3

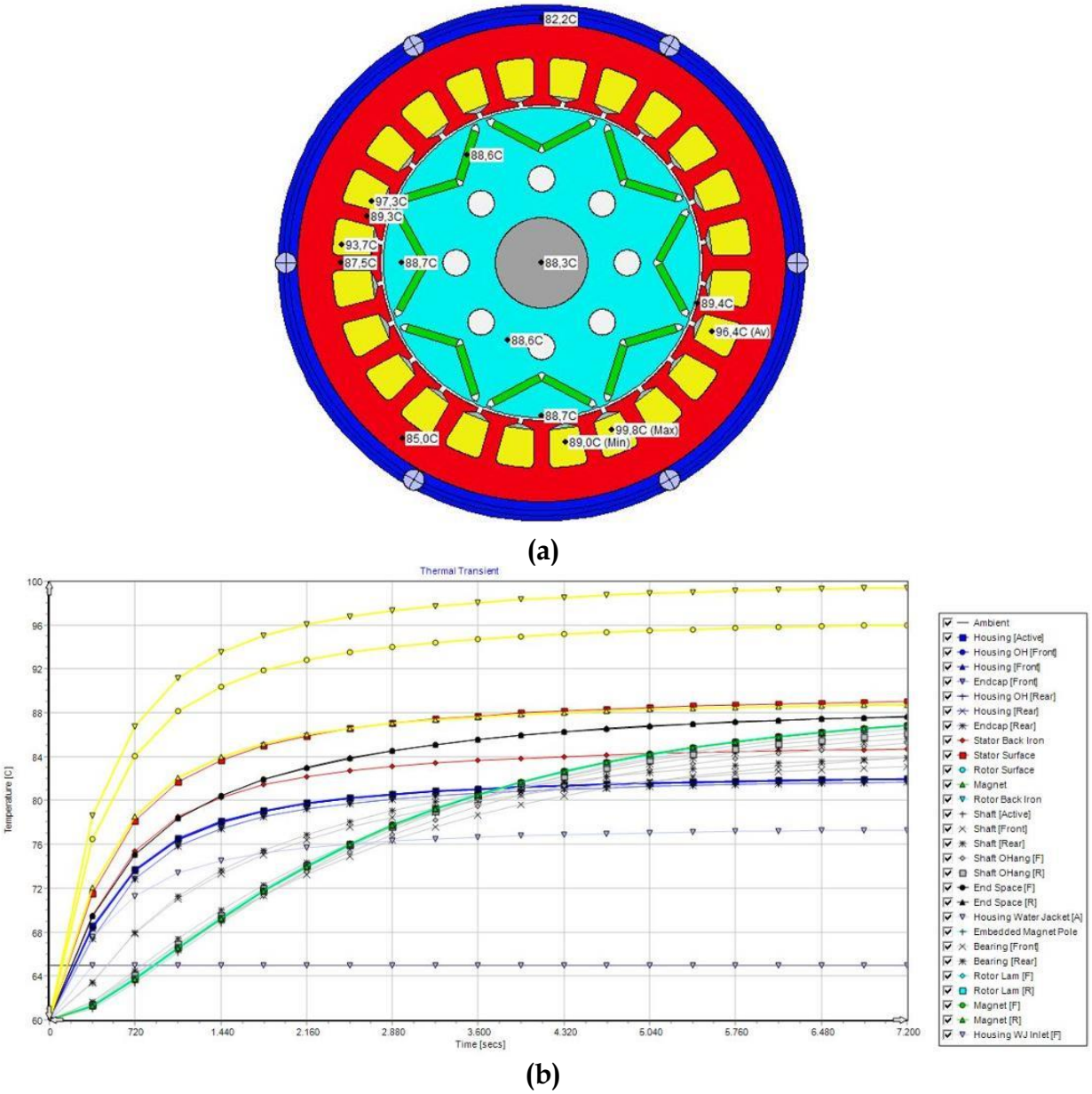

Figure 10. Thermal solution of IPM motor; (a) Steady-state solution, (b) Transient solution.

5. CONCLUSION

In this paper, the design details of an IPM motor are presented and the rated parameters of the IPM motor are determined. The parameters of the IPM motor are designed as follows: 24 slots, 8 interior V magnets, 35 Nm of torque, 1500 Watt, 72 line-line volts, and 40 Amps. Then, the formulas that are needed to determine the dimensions of the designed IPM motor are given. Whether the parameters of PMSM IPM motor is suitable for production or not is examined in detail with MotorCad motor design program. It is determined that the magnetic analysis does not saturate. The torque, power, and speed of the IPM motor are observed at the desired level. It is

determined that extra optimization is required because the knock torque is high. For this, it is necessary to give a slope to the stator. This is not held in this paper as it would make mechanical production stage difficult. The obtained thermal results shows that the designed IPM motor operates with an efficiency of around 92% even under extreme operating conditions.

REFERENCES

[1] F. L. Pope The Inventions of Thomas Davenport. Transactions of the American Institute of Electrical Engineers Jan. 1891; vol. VIII; no. 1; pp. 93-97.

[2] Chapman, Stephen J Electric Machinery Fundamentals. 1991.

[3] P. Pillay and R. Krishnan, "Modeling, simulation, and analysis of permanent-magnet motor drives. II. The brushless DC motor drive," in IEEE Transactions on Industry Applications, vol. 25, no. 2, pp. 274-279, March-April 1989, doi: 10.1109/28.25542.

[4] Z. Q. Zhu and D. Howe, "Electrical Machines and Drives for Electric, Hybrid, and Fuel Cell Vehicles," in Proceedings of the IEEE, vol. 95, no. 4, pp. 746-765, April 2007, doi: 10.1109/JPROC.2006.892482.

[5] Yılmaz M. Limitations/capabilities of electric machine technologies and modeling approaches for electric motor design and analysis in plug-in electric vehicle applications. Renewable and Sustainable Energy Reviews, 2015; 52; 80–99.

[6] Fitzgerald, A E, Charles Kingsley, and Stephen D. Umans Electric Machinery. 2003.

[7] T. M. Jahns, "Flux-Weakening Regime Operation of an Interior Permanent-Magnet Synchronous Motor Drive," in IEEE Transactions on Industry Applications, vol. IA-23, no. 4, pp. 681-689, July 1987, doi: 10.1109/TIA.1987.4504966.

[8] K. T. Chau, C. C. Chan and C. Liu, "Overview of Permanent-Magnet Brushless Drives for Electric and Hybrid Electric Vehicles," in IEEE Transactions on Industrial Electronics, vol. 55, no. 6, pp. 2246-2257, June 2008, doi: 10.1109/TIE.2008.918403.

[9] H. Le-Huy, R. Perret and R. Feuillet, "Minimization of Torque Ripple in Brushless DC Motor Drives," in IEEE Transactions on Industry Applications, vol. IA-22, no. 4, pp. 748-755, July 1986, doi: 10.1109/TIA.1986.4504787.

[10] Z. Q. Zhu, D. Howe, E. Bolte and B. Ackermann Instantaneous magnetic field distribution in brushless permanent magnet DC motors. I. Open-circuit field. IEEE Transactions on Magnetics, Jan. 1993; vol. 29; no. 1; pp. 124-135.

[11] Z. Q. Zhu and D. Howe Analytical prediction of the cogging torque in radial-field permanent magnet brushless motors. IEEE Transactions on Magnetics March 1992; vol. 28; no. 2; pp. 1371-1374.

[12] K. Kim, K. Kim, H. J. Kim and J. Lee, "Demagnetization Analysis of Permanent Magnets According to Rotor Types of Interior Permanent Magnet Synchronous Motor," in IEEE Transactions on Magnetics, vol. 45, no. 6, pp. 2799-2802, June 2009, doi: 10.1109/TMAG.2009.2018661.

[13] Buhr, K., & Voženílek, P. (2012). Analysis of an Electric Vehicle with a BLDC PM Motor in the Wheel Body. Transactions on Transport Sciences, 5(1), 1-10. doi: 10.2478/v10158-012-0001-8.

[14] Hanselman, Duane C. Brushless permanent-magnet motor design, 1994.